X

Scour in Stormwater Catchbasin Devices – Experimental Results from a Full-Scale Physical Model

Humberto Avila and Robert Pitt

X.1 Introduction

Hydrodynamic devices have long been proposed as sediment traps in storm drainage systems. The earliest, and simplest, hydrodynamic device is an inlet with a catchbasin sump (Lager *et al.* 1977). Early use of these devices has been to act as a trap to capture large debris, minimizing their deposition in the storm drainage system. Moreover, a number of research studies have investigated the performance of catchbasins as stormwater quality control devices by evaluating their sediment and pollutant removal capacities (Lager, *et al.* 1977, Pitt 1979, 1985, 1994, 1998, and 1999, Aronson, *et al.* 1983, and Butler, *et al.* 1995). Currently, sediment scour is a major subject of concern when evaluating the performance of catchbasins and related hydrodynamic separators in stormwater systems, and when developing protocols for scour evaluation, such as being examined by the Wisconsin Department of Natural Resources (WDNR) (Brzozowski 2006).

A series of experiments have been conducted at the University of Alabama over the past few years to evaluate sediment scour potential in stormwater catchbasins. Two types of experiments were performed with a full-scale physical model as part of these tests: 1) a hydrodynamic test

where velocities were measured at different locations in the control volume of the catchbasin and for different flow rates and inlet geometries, and 2) a scour test where turbidity, particle size distribution, and total suspended solids at the outlet were measured for different conditions of sediment depth and flow rates. The experimental results presented in this paper show the effect of two different inlet geometries (rectangular and circular) on the velocity field in the control volume, the benefit of the overlaying water in protecting the sediment from being scoured, the scour behavior under the effect of sediment armoring, and the mass losses of scoured sediment under varied flow conditions, among other findings. These results will be used to calibrate and validate a three-dimensional Computational Fluid Dynamics (3D-CFD) model that can simulate a variety of scenarios and geometries to determine the scour mass and pattern under different conditions. This paper is complementary to the previous publication (Monograph 16) on which the factors affecting scour of pre-captured sediment from catchbasin sumps were evaluated (Avila, *et al.* 2008). This paper extends that initial discussion by presenting the results of the field tests of scour from catchbasin sumps.

X.2 Methodology

A full-scale physical model was built with a maximum flow capacity of 10 L/s. The model consists of a catchbasin sump 116 cm in diameter and a trailer equipped with a frame, a channel (inlet), a pump and two flow meters. Two different experiments were performed: 1) hydrodynamic tests with velocities in x, y and z directions measured with an Acoustic Doppler Velocity Meter (FlowTracker Handheld ADV, Sontek) at 155 different locations within the control volume distributed on 5 layers with 31 points each (Figure X.1). Three flow rates (2.5, 5.0, and 10 L/s) and two types of inlet geometries (50 cm-wide rectangular inlet, and 30 cm circular pipe inlet) were evaluated, and 2) a scour test, during which turbidity time series, suspended sediment concentration (SSC), and Particle Size Distributions (PSD) were measured at the outlet of the catchbasin. For this test, a sediment mixture was prepared, based on the PSD of pre-deposited sediment in catchbasins found by Valiron and Tabuchi (1992) and Pitt and Khambhammuttu (2006). The sediment mixture was placed at four depths: 10, 25, 46, and 106 cm below the

outlet (Figure X.2) for each test series; the scour test was performed with five successive steady flow rates (0.3, 1.2, 3.0, 6.2, and 10.0 L/s) and four impacting tests of 10 L/s each. The scour tests were performed at Lake Lureen at Lake Lureen State Park, Northport, AL, as once-through tests using the lake water. The catchbasin effluent was directed to a large pool to settle any scoured material before the water was redirected back to the lake.

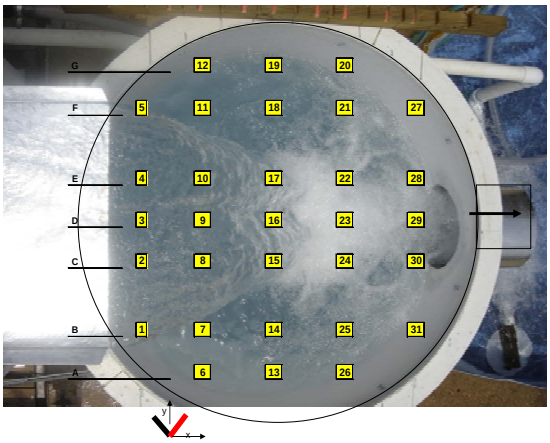

Figure X.1. Plan view of a layer with 31 points for measuring velocities. Velocity was measured at 5 different elevations.

Figure X.2. Placement of sediment at 25 cm below the outlet (left). Performing scour test (right).

The geometry of the catchbasin was based on the optimal geometry recommended by Lager, *et al.* (1977), and tested by Pitt (1979, 1985, and 1998). For this geometry, if the outlet diameter is D, the total depth of the catchbasin sump is 6.5D and the inside diameter is 4D; the outlet has to be located 4D above the bottom and 2.5D below the top of the catchbasin. The outlet diameter (D) was selected as 300 mm (12 inches) for the physical model. The full-scale physical model had a maximum flow capacity of 10 L/s available for the tests (see Figure X.3).

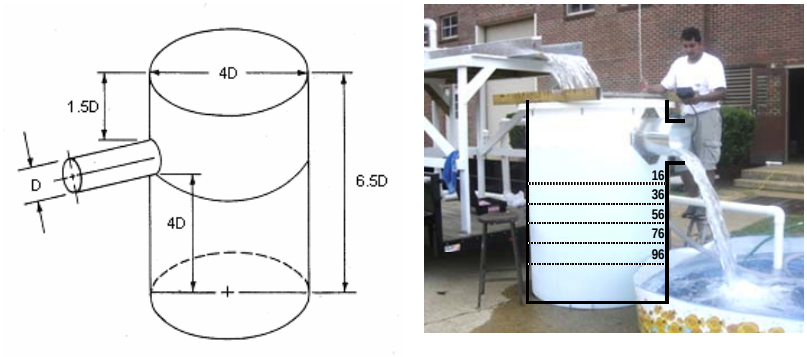

Figure X.3. Optimized catchbasin geometry by Lager, et al. (1977) (left). Full-scale physical model showing the depths below the outlet where the velocity measurements were taken during the recirculating water tests (right).

X.3 Hydrodynamic Results

X.3.1 Probability distributions of measured velocities

Velocity magnitudes and direction, obtained from the hydrodynamic tests, showed the effect of the plunging water jet on the control volume. It was possible to identify the velocity pattern at different elevations using different inlet geometries for a range of flow rates between 2.5 and 10 L/s. Figure X.4 for example, compares the mean z-velocities (vertical water motion) at 36 and 96 cm below the outlet using a 50 cm-wide rectangular inlet with a 10 L/s flow rate. The figure shows that for most locations at 96 cm below the outlet, the z-velocities are considerably smaller than the velocities at 36 cm below the outlet. Additionally, it is possible to see that there is an important ascending component at 36 cm

below the outlet with velocities up to 8.0 cm/s at point 29 which is located close to the outlet.

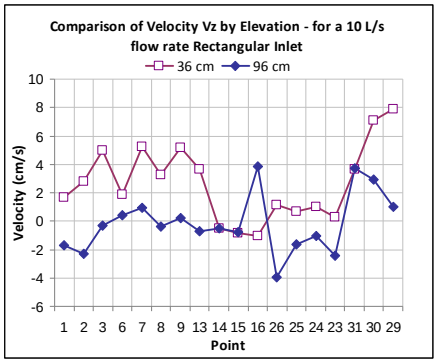

Figure X.4. Comparison of mean z-velocities on different points located at 36 and 96 cm below the outlet. Test performed with a rectangular inlet and 10 L/s flow rate.

It is important to consider not only the mean velocity, but also its variation. Figure X.5 shows the normal probability plot of z-velocities at 36 and 96 cm below the outlet at point 16 (located in the center of the projected top area of the control volume). This figure shows that at 36 cm below the outlet, the mean z-velocity is -1.0 cm/s with a standard variation of 3.3 cm/s, while at 96 cm below the outlet, the z-velocity is 3.8 cm/s with a standard variation of 3.1 cm/s. Both probability plots indicate likely normality with a p-value of 0.47 and 0.37 for the 36 and 96 cm elevations, respectively. The Anderson-Darling test compares the data to a normal distribution; a high p-value indicates that a significant difference between the data and the normal probability distributions could not be detected for the number of data points available. All the probability plots of velocity were likely normally distributed.

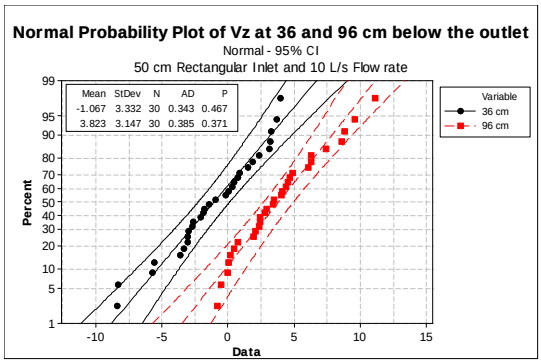

Figure X.5. Normal probability plots of z-velocities at 36 and 96 cm below the outlet at point 16. Scenario with rectangular inlet and 10 L/s flow rate.

The probability plots of the experimental velocities were compared to simulated data from a 3D-CFD model implemented in Flow-3D (Flow Science, 2007) at several points located in the control volume. The mean and variations of the velocities were of greatest interest during these comparisons.

X.3.2 Effects of flow rates and overlaying water depths on velocity distributions in the control volume

The effects of flow rate and overlaying water depth on the velocity magnitudes at different elevations in the control volume were determined for a variety of test conditions. The maximum velocity magnitudes of Vx, Vy, and Vz measured at each elevation were plotted to summarize the values of 4,650 velocity measurements taken during each flow rate test (Figure X.6). The measured velocities in the x-direction showed that as the flow rate increased, the x-velocities also increased significantly; and as the overlaying water depth increased, the x-velocities tended to decrease, all as expected. The x-velocities measured at 36 cm below the outlet, and lower, are not considerably different, with maximum x-velocities of about 40 cm/s observed during the 10 L/s flow rate test. However, at 16 cm below the outlet, the maximum x-velocities reached 140 cm/s, showing that when the water depth increased from 16 cm to 36 cm below the outlet, the maximum x-velocity magnitudes were reduced by 3.5 times. This data also shows that the turbulent zone caused by the plunging water jet reaches below 36 cm beneath the outlet, although its

effects at these depths are much less than for shallower depths. The same behavior was observed for the maximum y-velocities, with about 20 cm/s at 36 cm below the outlet, and 40 cm/s at 16 cm below the outlet, during the 10 L/s tests.

The maximum magnitudes of z-velocities also increased as the flow rate increased; however, in contrast to the x and y-velocity magnitudes, increasing overlaying water depths greater than 36 cm had an increasing effect in reducing the maximum observed z-velocities, especially at high flow rates. For example, Figure X.6 shows that at 10 L/s flows, the maximum z-velocity magnitude was reduced from 250 cm/s at 16 cm below the outlet, to 80 cm/s at 56 cm below the outlet, and to 25 cm/s at 96 cm below the outlet. However, under low flow rates, the differences between layers below 36 cm below the outlet were not significant. This can be explained by the large amount of entrained air during the high flow rate tests. As the flow rates increased, the turbulence created by the plunging jet is higher, contributing to greater air entrainment which causes an ascending velocity component due to buoyancy.

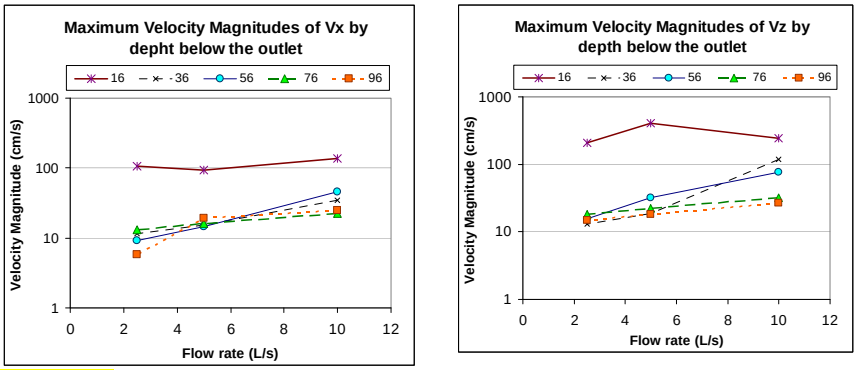

Figure X.6. Maximum magnitudes of x-velocities (left), and z-velocities (right) by elevation below the outlet as a function of flow rate. Rectangular Inlet.

X.3.3 Effects of inlet geometry on observed velocities in the control volume

Two different inlet geometries were evaluated during the full-scale physical model tests. A 50-cm rectangular inlet representing typical

gutter flows and a 30-cm diameter pipe inlet representing in-line installations. The comparison of the effects of both inlet geometries on the velocity field in the control volume was done by comparing the measured maximum velocity on each layer for each velocity component (x, y, and z). The results showed that the circular inlet, compared to the rectangular inlet, is associated with larger observed velocities in the velocity field, increasing the velocities in all three directions (especially close to the surface) (Figure X.7). Avila *et al.* (2008) evaluated the shear stresses at different elevations produced by a rectangular and circular inlet using a 2D-CFD model implemented in Fluent 6.2 (ANSYS, 2007). The results showed that the circular inlet generates significantly higher shear stress magnitudes at all overlying water depths than with a rectangular inlet, and therefore likely causes increased scour of previously captured sediment.

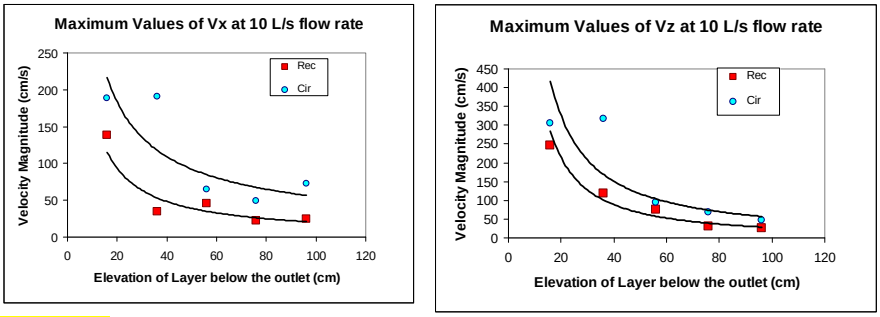

Figure X.7. Maximum magnitudes of x-velocities (left) and z-velocities (right) by inlet geometry as a function of elevation below the outlet. Scenario at 10 L/s flow rate.

Another finding is illustrated in Figure X.7: the exponential reduction of the velocity magnitudes as a function of the overlaying water depth. This decrease in velocity is more significant at high flow rates, as was previously mentioned.

X.4 Scour Results

X.4.1 Particle size distribution of previously captured sediment

A sediment mixture was prepared having a particle size distribution (PSD) similar to the measured values from previously captured sediment sampled from catchbasin sumps, as observed by Valiron and Tabuchi (1992), and Pitt and Khambhammuttu (2006). The characteristic diameters of this sediment mixture are D_{10} = 90 µm, D_{50} = 500 µm, and D_{90} = 2,000 µm (Figure X.8, which also shows the particle size distributions for the separate components used to make the mixture and the actual final mix used).

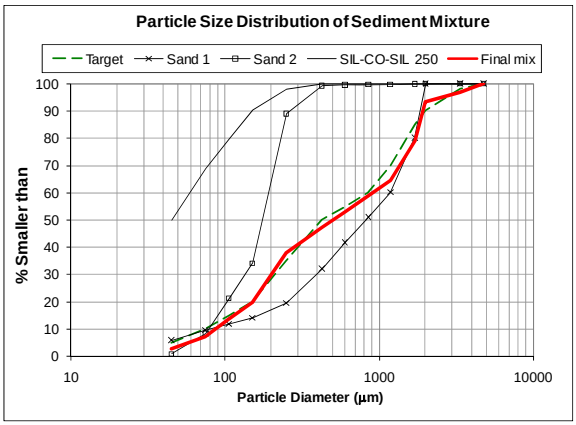

Figure X.8. Particle Size Distribution (PSD) of sediment mixture prepared for scour test.

This wide distribution of sizes of particles in sediment in the sump contributes to the effects of bed armoring. Bed armoring is the development of an erosion-resistant surface layer of relatively large particles created by the preferential scour of fine particles from the surface layers. Future very large, or intermittent, flows may in turn disturb this initial bed armoring layer, exposing a fresh supply of finer material that can be preferentially scoured, creating a new, and deeper, bed armoring layer. Eventually, the surface becomes relatively stable under almost all flow conditions expected, with minimal additional scour.

There are different types of armoring that can occur in catchbasin sumps. Some include: 1) armoring caused by the presence of leaves, plastics, or other non-sediment relatively flat material deposited on the

sediment surface which protect the underlying sediment (these can be incorporated as distinct reinforcing layers in the sediment, protecting the underlying material), 2) armoring caused by the presence of clay soil in the pre-deposited sediment which is characterized by the hardening of the sediment surface over time (however, this effect is most significant when the sediments are allowed to dry to form a hardpan, not likely with catchbasin sumps with overlying water), and 3) armoring caused by the accumulation of relatively large sediment particles on the surface of the sediment that are resistant to erosion (caused by the removal of the fines near the surface). The results presented in this paper only address the third type of armoring. Field observations of catchbasin sump accumulations over extended periods by Pitt (1979, 1983, and 1986) found that this third armoring mechanism was most significant. During these western tests, leaves and other bulky materials tended to accumulate on the surface of the natural catchbasin sediments, but were readily washed out of the sump during subsequent events due to their low specific gravity and large areas.

X.4.2 Scour behavior reflected by turbidity measurements

Turbidity concentration time series were recorded at the outlet for all the tests using a time increment of 30 sec. Even though turbidity could not be directly related to particle sizes or particulate mass, it did reveal the scour pattern for different flow rates and overlying water depths above the sediment.

The turbidity time series showed that with this specific sediment PSD, the scour had a negative exponential pattern under steady flow conditions, having a maximum turbidity value at the beginning of the flow when the plunging impact of the incoming water had its greatest effect, and decreasing exponentially over time. This pattern was more evident when the sediment was located relatively close to the outlet (with shallow water layers over the sediment) where it is more exposed to scour. With sediment at 10 cm below the outlet for example (Figure X.9), the negative exponential pattern is clear even at flows as low as 0.3 L/s. However, when the flow rate increased, peak turbidity values also increased: the peak turbidity values were proportional to the flow rate. The turbidity values decreased exponentially over time as the small

particles on the surface sediment layer were washed out and bed armoring was formed. This pattern was consistent for all the evaluated flow rates. The maximum turbidity value obtained was over 1,000 NTU during the 10 L/s flow rate tests.

When the sediment was located at 25 cm below the outlet, the peak turbidity values were not as high, nor was the exponential decaying pattern as evident, for the low flow rates (0.3 and 1.3 L/s). For the low flows, the velocity field created was not sufficient to cause significant scour. However, once the flow rate increased to 3.0 L/s, the turbidity exponential decaying pattern was again evident. The maximum turbidity value at 10 L/s flow rate was only 100 NTU when the overlying water was 25 cm deep, which is approximately 10 times less than when the overlying water depth was only 10 cm over the sediment. With sediment at 46 cm below the outlet, the pattern was barely evident at 6.3 L/s flow rate, and a maximum turbidity value of only 20 NTU was obtained at 10 L/s. At 106 cm below the outlet, the pattern was not evident for any flow condition, and the effluent turbidity values were never greater than 5 NTU.

These results illustrate the significant benefit associated with the overlaying water layer in protecting the previously captured sediment in the catchbasin sump, even under the severe conditions associated with the velocity field created by an aerated plunging water jet.

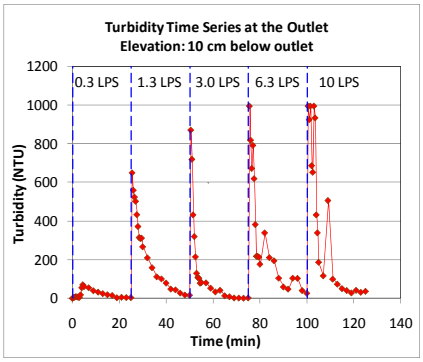

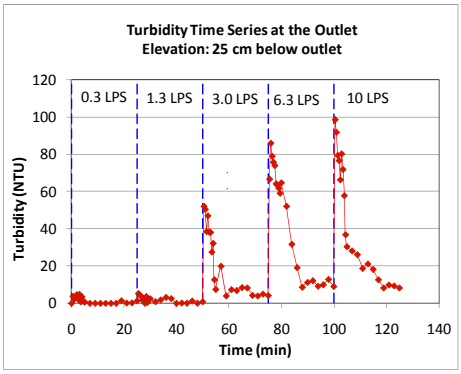

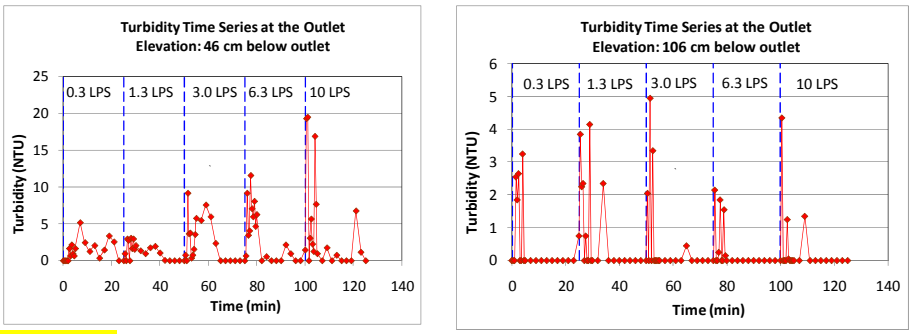

Figure X.9. Turbidity time series at the outlet for scour tests. 10 cm (top left). 25 cm (top right), 46 cm (bottom left), and 106 cm (bottom right) overlying water depths above the sediment and below the outlet (note differences in turbidity scale values).

X.4.3 Armoring effect on reducing sediment scour

The turbidity time series tests showed that an armoring layer of large sediment particles is formed on the sediment surface during steady flow conditions. This finding reveals that if relatively large particles (D_{75}=1,500 μm, D_{90}=3,350 μm, and D_{max}=4,750 μm for this experiment) are present in the pre-deposited sediment in a catchbasin sump, the scour potential of underlying smaller particles is rapidly decreased as an armoring of the larger particles rapidly form on the sediment surface; therefore, only a few centimeters of the surface sediment will be exposed to scour. However, the effectiveness of the armoring is relative to the fraction or proportion of large particles in the pre-deposited sediment and their proximity to the sediment surface.

Two processes may be occurring, either separately or simultaneously: 1) preferential washing of small particles from the voids around the larger particles. Shear stress defines the size that will remain behind, and exposed particles smaller than this size are removed, until a complete armoring layer of the large particles remains behind, protecting any underlying smaller particles, 2) a “wash machine” effect occurs where the surface layer is tumbled about; the largest particles that can be suspended is also dependent on the shear stress. As this mixture moves about, smaller particles can be transported out of the system before they can resettle to the sediment layer, leaving behind the larger ones that then

settle back down as the flow decreases, forming a protecting layer over the underlying sediment. The depth of the sediment that can be disturbed like this is likely dependent on the shear stress and carrying capacity of the water.

The turbidity time series presented above in Figure X.9 only showed the scour pattern under steady flow rates, in increasing increments, but not under rapidly fluctuating conditions at the same flow. Therefore, a fluctuating flow test was performed, applying four successive flows of 10 L/s, each lasting 3 min. Each flow was stopped at 3 min and immediately re-started to create the next flow burst. Thus, a total of four flow bursts were applied and the total effective flow time was 12 min. Figure X.10 shows the resulting turbidity time series for all the tests conducted with different overlying water depths during the series of impacting flow tests.

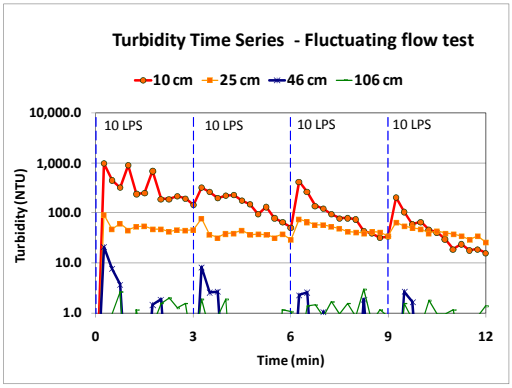

Figure X.10. Turbidity time series at the outlet for the series of impacting tests using short durations of 10 L/s flows.

The turbidity values reached a peak every time the plunging jet impacted the water with the shallow 10 cm overlying water depth and successive short duration flows of 10 L/s,. However, the peak values decreased with each successive flow, from 1,000 NTU at the first impact to 200 NTU at the forth impact, showing that armoring is gradually protecting the sediment bed, even from fluctuating flows that are likely during an actual runoff event. Also, with the shallow water depth, the turbidity time series still exhibited an overall negative exponential

pattern, with decreasing turbidity values during the short flow durations. A similar, but less dramatic scour pattern was obtained when the overlying water depth above the sediment was increased to 25 cm; the maximum turbidity values were much less, about 90 NTU for the first impact and 64 NTU for the forth impact. However, when the water depth was increased to 46 cm above the sediment, the initial turbidity peak was only 20 NTU, and decreased to maximum initial turbidity peaks of only about 5 NTU for the last two impacts. With a water layer depth of 106 cm above the sediment, no evident pattern was detected and the turbidity values were always below 5 NTU.

These findings show that sediment is more sensitive to scour under fluctuating than under long-term steady flow conditions. Additionally, the results also show that armoring is also formed relatively rapidly during fluctuating flow conditions, effectively protecting the underlying sediment from scour even under the impacting plunging water jets. During these tests, armoring was seen to form within a few minutes. The turbidity decreases as the number of impacts of flow at the same rate increases. Sediment scour is therefore highest during the initial stage of a runoff event, even if the flows keep increasing. After a few minutes at the peak runoff rate for the event, sediment scour substantially decreases as the armoring is formed at the sediment surface. Subsequent runoff events may have greatly reduced scour, unless new flows are large enough to disturb the armoring layer material. Besides large particles, other materials may help form armoring of the sediment surface, including leaves, clay soil, and other debris, if they accumulate on the sediment surface in the sump. However, if the water depth over the sediment is large (such as the 46 cm depth during these tests), the benefits of armoring are significantly decreased, as very little scour is likely to occur (at least at the 10 L/s, or less, flow rates tested).

X.4.4 Particle Sizes Exposed to Scour

Particle size distributions in the effluent water were determined for each flow rate and overlying water depth test. An initial effluent water sample was collected as a composite during the first 5 minutes of flow, and a second composite sample was collected over the next 20 minutes of flow, covering the entire 25 minutes of each test. This resulted in 125

min of successively increasing flows, from 0.3 L/s to 10 L/s, for each sediment depth setup. The particle size distributions were determined by wet sieving through successive sieves: 2000, 1200, 425, 250, 150, 106, 45, 32, and 20 μm. The wet sieve analysis was performed with 10 subsamples of 100 mL, each obtained from splitting a 1.0 L composite effluent sample with a USGS/Decaport cone water sample splitter. The particle size information of the lake water was subtracted from the effluent sample observations to remove the background effects.

Table X.1 summarizes the particle size distributions for both the 5-min and 20-min composite samples for each flow rate and water layer depth over the sediment. The table shows the particle sizes for the 50th and 90th percentiles, plus the maximum scoured particle size observed in the effluent water.

Table X.1. Summary of Particle Size Distribution (PSD) for the 5-min and 20-min composite samples.

Water Layer Depth over Sediment (cm)	Flow rate (L/s)	Percentile					
		5-min Composite Sample			20-min Composite Sample		
		50th (μm)	90th (μm)	Max (μm)	50th (μm)	90th (μm)	Max (μm)
10	0.3	< 20	150	1200	45	150	1200
	1.3	20	150	1200	45	200	1200
	3.0	45	200	1200	106	200	1200
	6.3	106	425	4750	150	1200	4750
	10.0	1500	3200	4750	1000	3000	4750
25	0.3	< 20	150	425	< 20	350	425
	1.3	< 20	250	425	250	300	425
	3.0	20	106	425	100	425	1200
	6.3	25	150	425	45	300	1200
	10.0	32	125	1200	106	425	1200
46	0.3	45	80	106	32	125	150
	1.3	45	250	425	45	400	425
	3.0	45	200	250	45	100	106
	6.3	45	106	150	32	106	425
	10.0	106	150	1200	32	150	1200
106	0.3	< 20	< 20	< 20	< 20	106	150
	1.3	32	40	45	32	40	45
	3.0	< 20	< 20	< 20	32	106	150

6.3	32	45	106	< 20	< 20	< 20
10	< 20	32	45	< 20	30	45

Figures X.11. and X.12., show the PSD plots for the different overlaying water depths (depth below the outlet) for the 6.3 L/s flow rate test for the 5-min and 20-min composite samples, respectively. The original PSD of the pre-deposited sediment is also included in the figures. The figures show that as the overlaying water depth increases, the proportion of large particles scoured decreases.

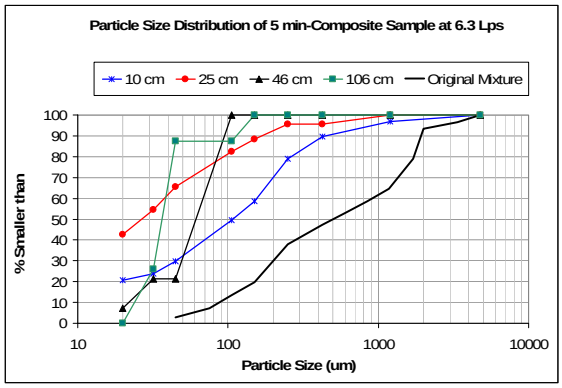

Figure X.11. Particle size distribution by depth of overlying water over the sediment for the 5-min composite sample at 6.3 L/s flow rate.

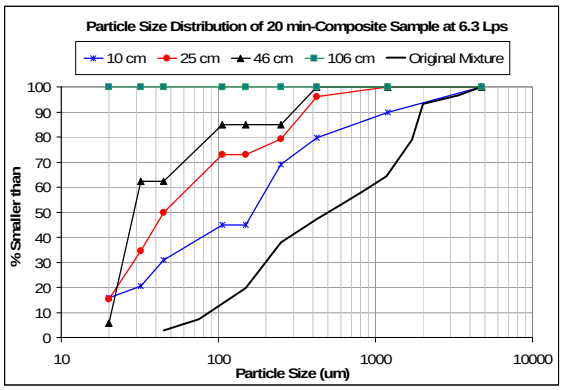

Figure X.12. Particle size distribution by depth of overlying water over the sediment for the 20-min composite samples at 6.3 L/s flow rate.

The observed maximum scoured particle size gives an indication of the significance of flow rate and overlaying water depth on the scour potential. Figures X.13 and X.14 show the maximum scoured particle sizes for the 5-min and 20-min composite samples. The figures show that the scour potential is directly proportional to the magnitude of flow rate and inversely proportional to the depth of water. During the first 5 min of flow for the 6.3 L/s flow rate test, for example, the maximum scoured particle size was 4,750 μm at 10 cm below the outlet, 425 μm at 25 cm below the outlet, 150 μm at 46 cm below the outlet, and 106 μm at 106 cm below the outlet.

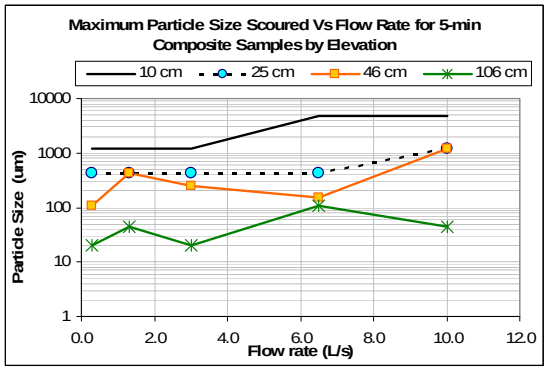

Figure X.13. Maximum scoured particle size as a function of flow rate for the 5-min composite sample. Values plotted by overlaying water depth below the outlet.

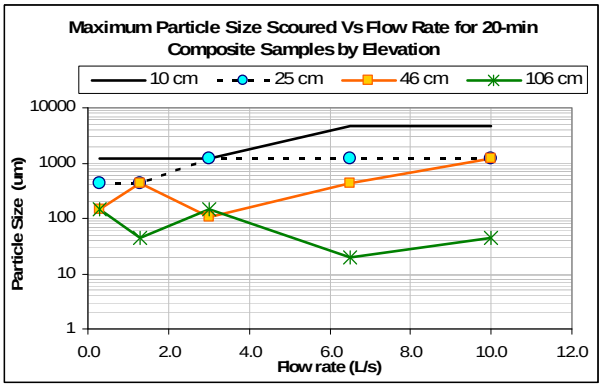

Figure X.14. Maximum scoured particle size as a function of flow rate for the 20-min composite sample. Values plotted by overlaying water depth below the outlet.

X.4.5 Scour-Mass Flux Rate

The sediment mass flux rate was calculated from the suspended sediment concentration (SSC) results. Tables X.2 and X.3 show the total scour-mass flux rates for the 5-min composite and the 20-min composite samples, respectively.

The scour-mass flux rates for different flow rates and overlaying water depths for the 5-min composite samples are shown on Table X.2. As the flow rate increases, the total mass-flux rate is also shown to increase, as expected. A maximum flux rate of 0.50 kg/min was measured when the overlying water layer over the sediment was 10 cm during the 10 L/s flow rate. The difference between the flux rate at 6.5 L/s (0.45 kg/min) and at 10 L/s (0.55 kg/min) is not large, considering that after 100 min of continuous flow before the 10 L/s flow rate was applied, an armoring layer was already formed. Therefore, it is possible that the flux rate for 10 L/s would actually be greater than shown here and would then decrease following the previously described exponential pattern.

Table X.2. Total mass-flux rate of scoured sediment for the 5-min composite samples.

	Flow rate (L/s)				
Depth below the outlet (cm)	**0.3**	**1.3**	**3.0**	**6.3**	**10.0**
	Total mass flux rate (gr/min)				
10	0.79	31	78	450	500
25	0.13	0.73	7.9	43	31
46	0.08	0.27	1.3	5.3	7.9
106	0.04	0.00	0.00	3.9	1.7

As the overlaying water depths increase, the mass-flux rate decrease exponentially. At the 6.3 L/s flow rate, for example, a flux rate of about 450 g/min was measured when an overlying water depth was only 10 cm,

but decreased to about 4.0 gr/min when the water depth over the sediment was increased to 106 cm. This is a sediment flux rate reduction of more than 100 times when the water depth increased by about 100 cm.

The pattern for the mass-flux rates for the 20-min composite samples is similar to the 5-min composite samples (Table X.3.). The flux rate increases exponentially as the flow rate increases for a given water depth; and as the overlaying water depth increases, the flux rate decreases exponentially for a given flow rate.

Table X.3. Total mass-flux rate of scoured sediment for the 20-min composite samples.

	Flow rate (L/s)				
Depth below the outlet (cm)	**0.3**	**1.3**	**3.0**	**6.3**	**10.0**
	Total mass flux rate (gr/min)				
10	0.31	4.82	7.3	97	440
25	0.03	0.45	3.9	9.3	13
46	0.06	0.08	0.95	6.2	7.6
106	<0.01	0.23	1.10	1.2	2.9

X.4.6 Total Scoured Sediment Mass

The total scoured sediment mass time series was based on the mass-flux rate, with the turbidity time series data used as weighting factors for each time increment. This sediment-mass time series was calculated for several particle size ranges and for the total scoured mass. The particle size ranges were: < 45, 45-150, 150-250, 250-425, 425-1200, and 1200-2000 μm. Each scoured mass time series is for a total period of 125 min, with five flow rate increments (for every 25 min). The flow rates examined were 0.3, 1.3, 3.0, 6.3, and 10 L/s.

Figures X.15 and X.16 show the scoured sediment mass time series categorized by particle size range for all tests. The flow rate is specified by a dashed line every 25 min. Figure X.15-top shows that particles as large as 1,200 mm were detected in the effluent at flow rates as low as 0.3 L/s. However, the sediment mass of particles in the range of 250 to 1200 μm is less than 0.4 gr over 75 min of flow. This mass may be associated with the initial impact in the first 5 min of flow. The scoured

sediment mass of these particles increased considerably when the flow was increased to 6.3 L/s, when particles as large as 4,750 μm were observed at the effluent for the shallow water tests.

Particles greater than 1,200 mm were not scoured when the water depth over the sediment was 25 cm for any flow rate tested (up to 10 L/s). However, particles within a size range of 425 to 1,200 mm were scoured at 3.0 L/s (Figure X.15-bottom).

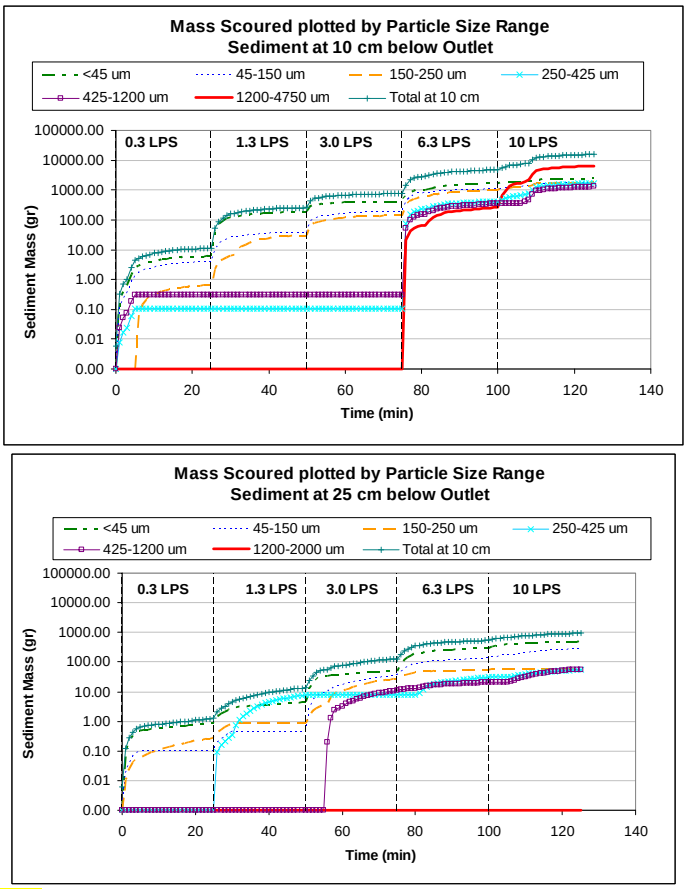

Figure X.15. Sediment mass scoured by particle size range for all the scour tests performed. 10 cm water depth over the sediment (top) and 25 cm water depth (bottom).

Figure X.16 shows the scoured mass time series when the water layer depth was 46 and 106 cm over the sediment. At 46 cm (Figure X.16-top), no particles larger than 1,200 µm were scoured at flow rates up to 10 L/s. Particles in the size range of 425-1,200 µm were scoured at 10 L/s. Particles smaller than 425 µm were also scoured at 1.3 L/s flow rate.

For water depths of 106 cm over the sediment (Figure X.16-bottom), only particles up to 45 µm were scoured with a significant mass of 135 gr over the 125 min duration of the test. However, even including particles up to 150 µm, their scour mass was very small (less than 0.001 gr).

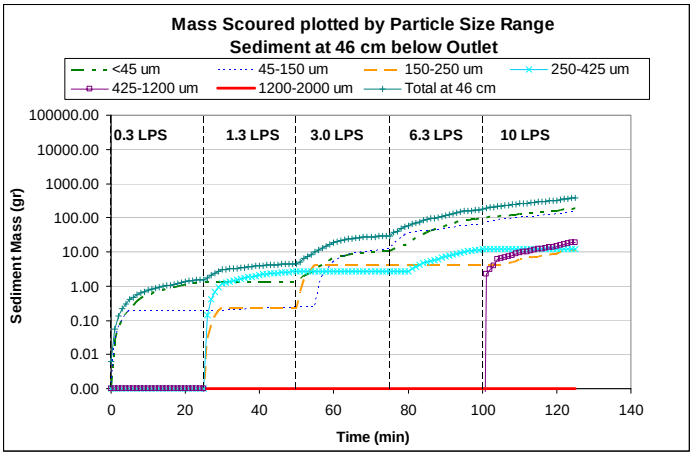

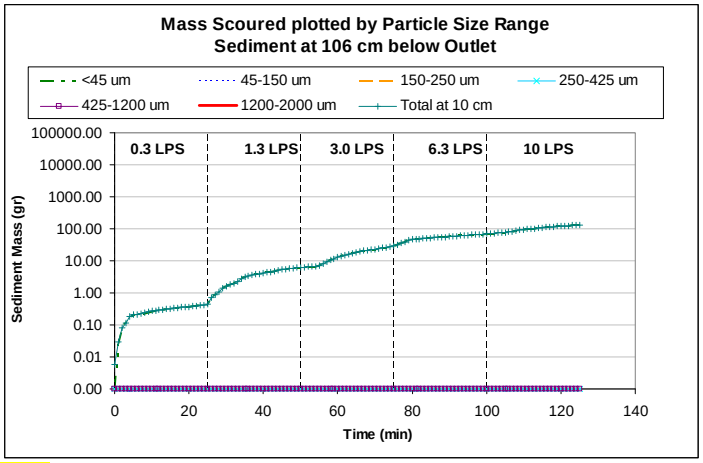

Figure X.16. Sediment mass scoured by particle size range for all the scour tests performed. 46 cm water depth over the sediment (top) and 106 cm water depth (bottom).

The total scoured mass time series presented in Figure X.17 shows that an increase in the overlaying water depth results in a significant reduction of the scoured mass of sediment. With an overlying water depth of 10 cm, the maximum scoured mass after 125 min was about 16 kg. The scoured particles were all smaller than 4,750 μm. This scoured mass is equivalent to a scour depth of about 0.9 cm in the catchbasin. In contrast, with an overlying water depth of 25 cm above the sediment, the total scoured mass after 125 min was reduced to less than 1 kg (930 gr), which is about 17 times less than observed with the 10 cm water layer. With an overlying water depth of 46 cm over the sediment, the total scoured mass was further reduced to only 360 gr in the 120 min period of flow. With a 106 cm water depth, the total scoured mass was reduced even further to only 134 gr during the 125 min test. With the deep water layer over the sediment, only particles smaller than 45 μm were observed in the effluent water.

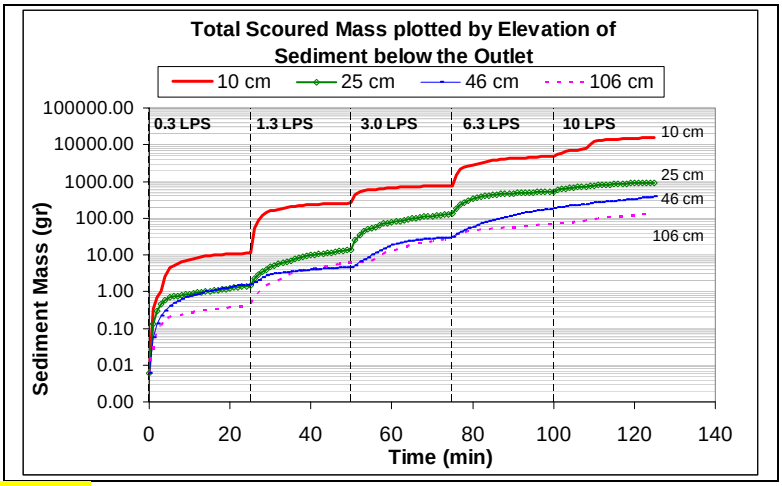

Figure X.17. Total sediment mass scoured by water depth over the sediment for all the scour tests performed.

Regression analyses were conducted to examine the effects of overlaying water depth and the scoured sediment mass. The depth of water was found to be a significant factor with a highly significant p-value of 0.006. A similar conclusion was also found in Avila *et al.* (2007) with CFD modeling. These results show that the overlaying water depth over the sediment significantly contributes to a reduction in scour potential. Moreover, even though armoring also contributes to a reduction in scour, its' benefits depend on the overlaying water layer depth. As the overlaying water depth increases, the armoring formation decreases because the sediment is less exposed to scour. However, at shallow overlaying water depths, the armoring layer plays an important role in reducing the scour potential. If no armoring mechanism is present at shallow overlaying water depths, the sediment scour will be considerably higher.

Recent experiments were conducted with a uniform particle size distribution to evaluate the scour potential with no armoring mechanism. The tests were conducted for two different water depths over the sediment: 25 and 34 cm below the outlet. Each test was performed with a 10 L/s flow rate for 30 min. These tests will be used to calibrate a 3D-CFD model implemented in Flow-3D to evaluate different scenarios and

obtain detailed results. It is anticipated that the findings from this analysis will be presented in the next edition of this publication series.

X.5 Conclusions

The following findings were concluded from this research:

These experimental hydrodynamic tests demonstrated that inlet geometry has a major effect on the velocity field in the control volume of a catchbasin. Circular inlets cause higher velocities in the control volume than rectangular inlets. This conclusion was also found by Avila, *et al.* (2008) and Faram, *et al.* (2003) using CFD modeling. This phenomenon is due to the smaller area associated with the impact zone as the plunging water strikes the water surface in the catchbasin, causing more concentrated power to be transferred to a smaller area of the pooled water.

The depth of the overlaying water on top of the sediment significantly reduces the scour potential in a catchbasin sump under free falling water jet conditions. This is especially true under high flow rates which generate more turbulence during impact with the water surface and increases the amount of entrained air. The ascending velocity component due to this added buoyancy also decreases the depth of the velocity field from the plunging water. The experimental results showed that the reduction of scour as a function of the overlaying water depth was exponential at 10 L/s flow rate.

Sediment armoring by large-sized particles is formed rapidly with time under steady flow conditions. This contributes to a layer of protection to the underlying smaller-sized sediment particles. Only the overlaying water will serve as a protection mechanism against scour if armoring is not present (due to the absence of the necessary larger particles or other large debris, such as leaves, or clay soil),.

The mass flux rate of scoured sediment increases exponentially with increasing flow rates and with decreases in overlaying water depths. Particles smaller than 4,750 μm were scoured when the overlying water depth above the sediment was 10 cm. A total mass of about 16 kg was scoured after 125 min of successively increasing flows up to 10 L/s. No particles larger than 1,200 μm were scoured when the overlying water depth was 25 cm above the sediment. A total mass of about 1 kg was scoured

under these conditions, decreasing to about 130 grams of sediment being scoured when the overlying water depth was 46 cm above the sediment. This suggests that for previously deposited sediment and with armoring, the maximum likely scour depth will be about 1.0 cm when the overlaying water depth is greater than 25 cm and when a maximum flow of 10 L/s is applied. This was visually verified during the full-scale scour tests.

Further experiments are being conducted with uniform particle size distributions to evaluate the scour mass for individual particle sizes under different conditions. 3D-CFD modeling analysis will also be conducted to evaluate additional scenarios.

References

Aronson, G., Watson d., and Pisano W. (1983). Evaluation of Catchbasin Performance for Urban Stormwater Pollution Control. U.S. EPA. Grant No. R-804578. EPA-600/2-83-043. 78 pages. Cincinnati, June.

Avila, H., R. Pitt, and S.R. Durrans. (2008). Factors affecting scour of previously captured sediment from stormwater catchbasin sumps. In: Stormwater and Urban Water Systems Modeling, Monograph 16. (edited by W. James, E.A. McBean, R.E. Pitt and S.J. Wright). CHI. Guelph, Ontario.

Brzozowski, C., (2006). BMP Testing Protocols: Wisconsin steps forward. Stormwater Journal. October.

Butler, D. and S.H.P.G. Karunaratne (1995). "The suspended solids trap efficiency of the roadside gully pot." Wat. Res. Vol. 29, No. 2. pp. 719-729.

Faram, M.; Harwood, R.; Deahl, P., (2003) "Investigation into the sediment removal and retention capabilities of stormwater treatment chambers," StormCon Conference, Texas, U.S. July.

Flow-3D v.9.2, Flow Science Inc. (2007). User's Manual. www.flow3d.com

Fluent 6.2. Computational Fluid Dynamic (CFD) Software. ANSYS, 2007. User's Manual. http://www.fluent.com/.

Lager, J.A., W.G. Smith, W.G. Lynard, R.M. Finn, and E.J. Finnemore. (1977). Urban stormwater management and technology: Update and Users' Guide. U.S. EPA-600/8-77-014", Cincinnati, U.S. September.

Metcalf & Eddy Inc., Lager J., Smith W., Tchobanoglous G., (1977). Catchbasin technology overview and assessment. U.S. EPA-600/2-77-051, Ohio, U.S.

Pitt, R. (1979)Demonstration of Nonpoint Pollution Abatement Through Improved Street Cleaning Practices. U.S. EPA. Grant No. S-804432. EPA-600/2-79-161. 270 pages. Cincinnati, August.

Pitt, R. and G. Shawley, (1982) A Demonstration of Non-Point Source Pollution Management on Castro Valley Creek. Alameda County Flood Control and Water Conservation District (Hayward, CA) for the Nationwide Urban Runoff Program. U.S. Environmental Protection Agency, Water Planning Division, Washington, D.C., June.

Pitt, R, (1985). Characterizing and Controlling Urban Runoff through Street and Sewerage Cleaning. U.S. EPA. Contract No. R-805929012. EPA/2-85/038. PB 85-186500/AS. 467 pages. Cincinnati, June.

Pitt, R., S. Clark, and K. Parmer, (1994). Protection of Groundwater from Intentional and Nonintentional Stormwater Infiltration. U.S. Environmental Protection Agency, EPA/600/SR-94/051. PB94-165354AS, Storm and Combined Sewer Program, Cincinnati, Ohio. 187 pgs. May.

Pitt, R., Field R, (1998). An Evaluation of Storm Drainage Inlet Devices for Stormawter Quality Treatment. Proc. Water Environmental Federation Technical Exposition - WEFTEC, Orlando, FL.

Pitt, R., B. Robertson, P. Barron, A. Ayyoubi, and S. Clark, (1999) Stormwater Treatment at Critical Areas: The Multi-Chambered Treatment Train (MCTT). U.S. Environmental Protection Agency, Wet Weather Flow Management Program, National Risk Management Research Laboratory. EPA/600/R-99/017. Cincinnati, Ohio. 505 pgs. March.

Pitt, R. and U. Khambhammettu. (2006), "Field verification tests of the UpFlowTM Filter (2006). Small Business Innovative Research, Phase 2 (SBIR2)" U.S. EPA, Edison, NJ, U.S. March.

Valiron F., Tabuchi J.-P. (1992) Maitrise de la pollution urbaine par temps de pluie. étatde l_art. Lavoisier, 564 pgs, ISBN 2-85206-863-X, París.